

Poly(Isobutylene-co-Isoprene) Composites for Flexible Electronic Applications

M.T. Sebastian and J. Chameswary

Abstract Flexible, bendable, and stretchable dielectrics which can cover even curved surfaces are important for applications in electronic control systems, consumer electronics, heart pacemakers, body-worn antenna, etc. The requirements for a material to be used as a flexible dielectric are good mechanical flexibility, low dielectric loss, high thermal conductivity (TC), low coefficient of thermal expansion (CTE), etc. It is very difficult to identify a single material which possesses all these properties simultaneously. There are a number of ceramic materials with high relative permittivity and low dielectric loss that are available but are brittle in nature. Butyl rubber has low dielectric loss with good mechanical flexibility and stretchability, but they have low relative permittivity, low TC, and high CTE. Therefore, the practical applications of an elastomer or a ceramic alone are limited. By integrating the flexibility, stretchability, and low processing temperature of butyl rubber with high relative permittivity and low loss of ceramics, a composite may be formed, which can deliver improved performances. In this review, the preparation, characterization, and properties of butyl rubber composites with several ceramics such as Al_2O_3 , BaTiO_3 on the microwave dielectric properties, thermal properties, moisture absorption, and mechanical properties are discussed.

Keywords Ceramics · Thermal properties · Dielectrics · Bending

M.T. Sebastian (✉)

Microelectronics and Materials Physics Laboratory, Department of Electrical Engineering,
University of Oulu, 90014 Oulu, Finland
e-mail: msebasti@ee.oulu.fi; mailadils@yahoo.com

J. Chameswary

Materials Science and Technology Division, CSIR-NIIST, Trivandrum 695019, India

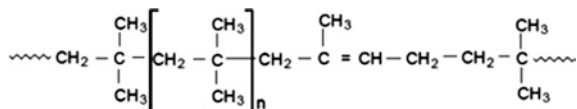
1 Introduction

Microwave dielectric materials play a key role in global society, with a wide range of applications from terrestrial and satellite communication to environmental monitoring via satellites. Recently, an increasing interest has been shown in the development of mechanically flexible electronic devices in various fields such as wireless communication, automotive, biomedical, and aerospace. For many applications, particularly in the biomedical field and body-worn antenna, electronic circuits are to be conformally wrapped around curved surfaces. In such systems, the circuits must be not only flexible but also stretchable. Flexible electronics is an emerging field in electronic industry which enable a wide range of applications such as capacitors for energy storage, wireless communication, electronic packaging, and electromagnetic interference (EMI) shielding. The development of EMI shielding materials is increasing in recent years in order to prevent the electromagnetic radiations emitting from modern electronic devices [1, 2]. Modern electronic industry requires systems that can be fitted into non-planar forms which can be folded and unfolded for packaging or storage [3, 4]. The flexible substrates have many potential applications from neural prosthetics in the medical field to microwave devices in electronics, which provides the advantage of three-dimensional designs of conformal structures [5, 6]. The requirements of a material to be used for flexible substrate applications are low relative permittivity, low loss tangent, low CTE, high TC, good mechanical flexibility, low moisture absorption, etc. Ceramics with optimum relative permittivity and low dielectric loss are available. But their brittle nature precludes them from practical applications in flexible electronics. Low-loss polymers with good flexibility are also available. However, their high CTE and low TC restrict their practical use. Hence, the use of polymers or ceramics alone is limited. The polymer–ceramic composites can deliver better performance than their constituent phases. There are several polymer–ceramic composites such as polytetrafluoroethylene (PTFE), polystyrene, polyether ether ketone (PEEK), and polyethylene with fillers such as silica, alumina, titania, and glasses, and some of these are commercially available. The reader is referred to the recent review by Sebastian and Jantunen [7] on polymer–ceramic composites for details. Conventional polymers filled with ceramic are rigid and cannot be bend or stretched. Stretchability means that the circuits should have the capacity to absorb large levels of strain without degradation in their electronic properties. In this context, the elastomer–ceramic composites can be used for stretchable and bendable electronic applications. However, not much attention was paid on bendable and stretchable materials such as elastomer–ceramic composites. In this chapter, we discuss the recent advances in low-loss butyl rubber–ceramic composites for microwave applications.

1.1 Butyl Rubber

Butyl rubber is a copolymer of 98 % polyisobutylene with 2 % isoprene distributed randomly in the polymer chain as shown in Fig. 1.

Fig. 1 Butyl rubber



Polymerization of isoprene results in the incorporation of a double bond or unsaturation into the polymer chain. These double bonds serve as cross-linking sites. Vulcanization of the butyl rubber with sulfur results in the formation of a network structure in the form of a cross-linked rubber. As such butyl rubber is a thermoset polymer and once vulcanized, it cannot be reformed into a new shape [8, 9]. Butyl rubber is amorphous and viscoelastic with low Young's modulus and high yield strain as compared to other polymer materials due to its weak intermolecular attractive forces. Butyl rubber exists above the glass transition temperature, and hence, considerable segmental motion is possible. The glass transition temperature of butyl rubber is around -63°C . At ambient temperatures, rubbers are relatively soft and deformable. The chain segments of elastomers can undergo high local mobility, but the gross mobility of chains is restricted by the introduction of a few cross-links into the structure. The long polymer chains cross-link during curing, and the process is known as vulcanization. The covalent cross-linkages ensure that the elastomer will return to its original configuration when the stress is removed. In the absence of applied stress, [10] molecules of elastomers usually assume coiled shapes. Consequently, elastomers exhibit large elongation (up to about 1000 %) from which they recover rapidly on removal of the applied stress.

Among elastomers, vulcanized butyl rubber has excellent dielectric properties, excellent heat/ozone resistance, high damping properties at ambient temperatures, mechanically flexible, air tight and gas impermeable, low glass transition temperature, good resistance to oxidizing chemicals, good weathering, and heat and chemical resistance. The main use of butyl rubber is in tyre-curing bladders and inner tubes and also used for seals, adhesives, and molded flexible parts [11–13]. These excellent properties of butyl rubber are the result of low levels of unsaturation between the long rubber chain segments. The molecular structure of butyl rubber can be oriented to resist stress, and thus, the mechanical properties are retained over a relatively wide stiffness range since reinforcement is not required for good tensile and tear strength [14].

Materials with varying relative permittivity are required for practical applications in electronic industry. Although butyl rubber is mechanically flexible and has excellent dielectric properties, it cannot be used for flexible electronic applications due to its low ϵ_r and poor thermal properties. The relative permittivity of butyl rubber can be tailored over a wide range by reinforcing with low-loss ceramics having different range of relative permittivity. For electronic packaging and substrate applications, materials must have a low relative permittivity to minimize capacitive coupling and signal delay along with low loss tangent to reduce signal attenuation. High-permittivity ceramic materials can be used to make butyl rubber composites for flexible dielectric waveguide and capacitor applications.

Table 1 Microwave dielectric properties of ceramics and butyl rubber [23]

Material	Relative permittivity (ϵ_r)	Loss tangent ($\tan \delta$)	CTE (ppm/°C)	TC ($\text{W m}^{-1} \text{K}^{-1}$)
Al_2O_3	10.1	1×10^{-5}	7.0	30.0
TiO_2	104.0	1×10^{-4}	9.2	11.0
SiO_2	3.8	1×10^{-4}	0.5	1.4
$\text{SrCe}_2\text{Ti}_5\text{O}_{16}$ (SCT)	113.0	1×10^{-4}	1.7	2.9
SrTiO_3	290.0	1×10^{-3}	9.4	12.0
$\text{Ba}(\text{Zn}_{1/3}\text{Ta}_{2/3})\text{O}_3$ (BZT)	28.0	1×10^{-4}	4.2	3.9
Butyl rubber	2.4	1×10^{-3}	191	0.13
BaTiO_3	>1500	1×10^{-2}	5.4	2.6
$\text{Ba}_{0.7}\text{Sr}_{0.3}\text{TiO}_3$	2850	1×10^{-2}	3.0	4.4

In addition, thermal properties of butyl rubber composites can be improved by the addition of ceramics, since ceramics have high TC and low CTE. Elastomer–ceramic composites can combine the advantageous properties of both elastomer and ceramics which can satisfy diverse requirements of present-day electronic industry. Today elastomer–ceramic composites found applications ranging from ultrathin health monitoring to advanced imaging devices. Although extensive researches were done on the microwave dielectric properties of rigid polymer–ceramic composites [7], very little attention was paid on elastomer–ceramic composites. Recently, we have reported the microwave dielectric properties of butyl rubber composites with SrTiO_3 , $\text{Sr}_2\text{Ce}_2\text{Ti}_5\text{O}_{16}$, SiO_2 , $\text{Ba}(\text{Zn}_{1/3}\text{Ta}_{2/3})\text{O}_3$, $\text{Ba}_{0.7}\text{Sr}_{0.3}\text{TiO}_3$, Al_2O_3 , BaTiO_3 , and TiO_2 composites [15–22]. The microwave dielectric properties of the ceramics used and butyl rubber are given in Table 1.

High-purity alumina has a very low loss tangent of about 10^{-5} . The very high TC ($30 \text{ W m}^{-1} \text{K}^{-1}$) and low CTE ($6\text{--}7 \text{ ppm}/^\circ\text{C}$) of alumina make it a suitable electronic packaging material [23]. Elastomer–alumina composites are well studied for its mechanical and curing characteristics [24, 25]. Silica is a low-permittivity ceramic with excellent dielectric properties ($\epsilon_r = 3.8$, $\tan \delta \approx 10^{-4}$) [26] and good thermal properties such as $\text{TC} = 1.4 \text{ W m}^{-1} \text{K}^{-1}$ and $\text{CTE} = 0.5 \text{ ppm}/^\circ\text{C}$. Silica is important reinforcing filler in elastomers for industrial applications. The effect of silica on dielectric properties of styrene-butadiene rubber was investigated by Hanna et al. [27] in the frequency range of $60\text{--}10^8 \text{ Hz}$ at room temperature. $\text{Ba}(\text{Zn}_{1/3}\text{Ta}_{2/3})\text{O}_3$ is a complex perovskite ceramic with $\epsilon_r = 28$, $\tan \delta \approx 10^{-4}$, and a nearly zero temperature coefficient of resonant frequency ($\tau_f = 1 \text{ ppm}/^\circ\text{C}$). BaTiO_3 is a ferroelectric material having relatively high permittivity greater than 1500 and does not resonate in the microwave frequency due to the high dielectric loss factor and has thermal properties such as $\text{TC} = 2.6 \text{ W m}^{-1} \text{K}^{-1}$ and $\text{CTE} = 6 \text{ ppm}/^\circ\text{C}$. Butyl rubber is a synthetic elastomer with excellent dielectric properties in the microwave frequencies ($\epsilon_r = 2.4$, $\tan \delta \approx 10^{-3}$), good mechanical flexibility, aging resistance, and weathering resistance [28].

2 Preparation of Butyl Rubber (BR)–Ceramic Composites

The raw materials of alumina, silica, and rutile were procured from Sigma-Aldrich. The SrCO_3 , BaCO_3 , and ZnO from Aldrich, Ta_2O_5 from Treibacher Industries, and CeO_2 from Indian Rare Earths Ltd. were used for preparing $\text{Ba}(\text{Zn}_{1/3}\text{Ta}_{2/3})\text{O}_3$ (BZT), $\text{Sr}_2\text{Ce}_2\text{Ti}_5\text{O}_{15}$ (SCT), SrTiO_3 , BaTiO_3 , and $\text{Ba}_{0.7}\text{Sr}_{0.3}\text{TiO}_3$ by conventional solid-state ceramic route. The stoichiometric amount of chemicals were mixed by ball milling and dried. The mixtures were then calcined followed by sintering at appropriate temperatures and ground well. The powders were sieved through a 25- μm sieve and then used for preparing butyl rubber–ceramic composites [15–22]. The nanoalumina (<50 nm particle size), nanorutile (100 nm), and nano- BaTiO_3 (100 nm) powders were purchased from Sigma-Aldrich, USA, and were used for preparing butyl rubber–nano composites in the present work. The nanopowders were dried at 100 °C for 24 h before use.

The butyl rubber used for present investigation was IIR grade. The process involving incorporation of ingredients such as activators, accelerators, vulcanizing agent, and fillers into the virgin rubber is known as compounding of rubber [15–22]. The compounding of butyl rubber mix was done by sigma blend method using a kneading machine. The butyl rubber was first masticated through the two counter rotating sigma blades in order to make it soft and more processable. Then, the additives are incorporated one by one as per the order given in Table 2. The additives such as zinc oxide and stearic acid act as activators for vulcanization, tetramethylthiuram disulfide acts as accelerator, and sulfur acts as vulcanizing agent. Finally, appropriate amount of ceramic filler was added. The mixing was done for about 30 min to get uniform composites. Thus, obtained composites were hot pressed at 200 °C for 90 min in suitable dies or molds under a pressure of 2 MPa. After hot pressing, the composites with desired shapes were used for characterization. The physical properties of butyl rubber are given in Table 3. In this review, we describe two representative materials, i.e., butyl rubber composites with alumina and barium titanate. Al_2O_3 is a very low-loss dielectric ceramic, whereas BaTiO_3 is ferroelectric ceramic with high relative permittivity and loss factor. Figure 2 shows the photograph of a typical butyl rubber–ceramic composite.

Since alumina is a widely used ceramic packaging material, the effect of filler particle size on dielectric, thermal, and mechanical properties of butyl

Table 2 Formulation of rubber mix [29]

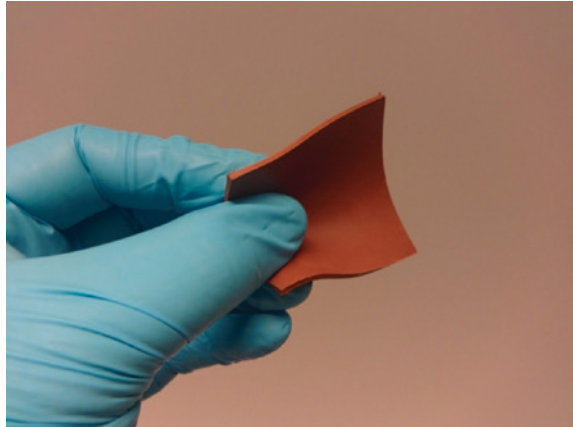
Ingredient	Loading (phr) [#]
Butyl rubber	100.0
Zinc oxide	5.0
stearic acid	3.0
Tetramethylthiuram disulfide	1.0
Sulfur	0.5

[#] parts per hundred

Table 3 Physical and electrical properties of butyl rubber [22]

Density	0.97 gcm ⁻³
Moisture absorption	0.039 vol.%
Relative permittivity at 5 GHz	2.4
Loss tangent at 5 GHz	≈10 ⁻³
Thermal conductivity	0.13 W m ⁻¹ K ⁻¹
Coefficient of thermal expansion	191 ppm/°C

Fig. 2 Photograph of butyl rubber–strontium cerium titanate ceramic composite

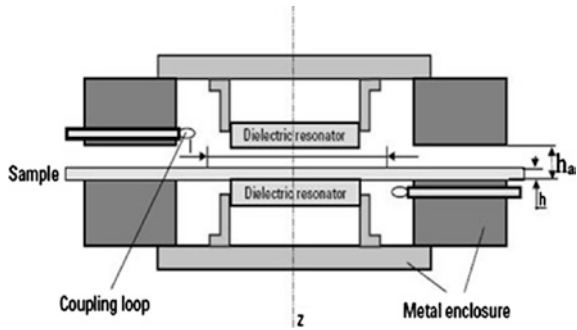


rubber–ceramic composites was studied in butyl rubber–alumina composites. The alumina (micron and nano) powders were dried at 100 °C for 24 h before using for composite preparation. The butyl rubber–micron alumina (BR/AL) and butyl rubber–nanoalumina (BR/nAL) composites were prepared as described earlier. The BR/AL composites were prepared with micron alumina loading up to a volume fraction (v_f) 0.42. The nanoalumina has high surface area and large ceramic volume. Hence, the possibility of agglomeration of nanoparticles increases with filler loading. This makes the processing of BR/nAL composites difficult at higher filler loading [30]. Hence, a maximum loading of 0.1 volume fraction of nanoalumina was possible in the case of BR/nAL composites. It was found that the use of coupling agent such as silane treatment although slightly improve the relative permittivity and mechanical properties degrades the microwave dielectric loss factor [22].

3 Dielectric Properties

The dielectric properties of the composites were measured in the radio frequency range by the parallel plate capacitor method employing a LCR meter and using thin pellets of about 1 mm thickness and diameter 11 mm. The dielectric

Fig. 3 Schematic representation of SPDR for microwave measurement [23]



properties at microwave frequency range were measured by the split-post dielectric resonator (SPDR) method. The SPDR is an accurate method for measuring the dielectric properties of substrates and thin films at a single frequency in the frequency range of 1–20 GHz [31–33]. In this method, the sample should be in the form of a flat rectangular piece or a sheet. The SPDR uses a particular resonant mode which has a specific resonant frequency depending on the resonator dimensions and the relative permittivity. The resonator mainly consists of two dielectric disks in a metal enclosure. The sample under test is placed in the gap between the two parts of the resonator. Figure 3 schematically shows SPDR fixture for the measurement of the relative permittivity of dielectric and loss tangent of sheet samples. SPDR usually operates with the TE_{01δ} mode. The relative permittivity of the sample is an iterative solution to the following equation [31]

$$\epsilon_r = 1 + \frac{f_o - f_s}{hf_o K_\epsilon(\epsilon_r, h)} \tag{1}$$

where h is the thickness of the sample under test, f_o is the resonant frequency of empty resonant fixture, f_s is the resonant frequency of the resonant fixture with dielectric sample, and K_ϵ is a function of ϵ_r and h and has been evaluated using Rayleigh–Ritz technique [32]. The loss tangent of the sample can be determined by

$$\tan \delta = (Q_u^{-1} - Q_{DR}^{-1} - Q_C^{-1}) / \rho_{es} \tag{2}$$

In Eqs. 1 and 2

$$\rho_{es} = h\epsilon_r K_1(\epsilon_r, h) \tag{3}$$

$$Q_c = Q_{c0} K_2(\epsilon_r, h) \tag{4}$$

$$Q_{DR} = Q_{DR0} \frac{f_o}{f_s} \cdot \frac{p_{eDR0}}{p_{eDR}} \tag{5}$$

where p_{es} and p_{eDR} are the electric energy filling factors for the sample and for the split resonator, respectively; p_{eDR0} is the electric energy filling factor of the

Table 4 Dielectric properties at 1 MHz and water absorption of BR/AL and BR/nAL composites [22]

Composite material	Sample designation	Filler in phr [#] (%) [§]	ϵ_r (1 MHz)	$\tan \delta$ (1 MHz)	Water absorption (vol.%)
Butyl rubber– micron alumina composite	BR-0	0 (0.00)	2.44	0.0003	0.039
	BR/AL-1	10 (0.02)	2.48	0.0011	0.045
	BR/AL-2	20 (0.04)	2.54	0.0012	0.045
	BR/AL-3	30 (0.06)	2.65	0.0021	0.056
	BR/AL-4	40 (0.08)	2.73	0.0032	0.057
	BR/AL-5	50 (0.10)	2.78	0.0046	0.065
	BR/AL-6	100 (0.26)	3.01	0.0051	0.067
	BR/AL-7	200 (0.33)	3.80	0.0063	0.071
Butyl rubber– nanoalumina composite	BR/nAL-1	10 (0.02)	2.49	0.0090	0.150
	BR/nAL-2	20 (0.04)	2.55	0.0110	0.220
	BR/nAL-3	30 (0.06)	2.67	0.0160	0.490
	BR/nAL-4	40 (0.08)	2.79	0.0270	0.620
	BR/nAL-5	50 (0.10)	2.81	0.0470	0.700

[#]Parts per hundred rubber

[§]The corresponding ceramic volume fraction is given in parenthesis

dielectric split resonator for empty resonant fixture; Q_{c0} is the quality factor depending on metal enclosure losses for empty resonant fixture; Q_{DR0} is the quality factor depending on dielectric losses in dielectric resonators for empty resonant fixture; and Q_u is the unloaded quality factor of the resonant fixture containing the dielectric sample. The values of p_{eDR} , p_{es} , and Q_c for a given resonant structure can be calculated using numerical techniques.

The sample should be flat and must be positioned such that it extends beyond the diameter of two cavity sections. The position of the sample in z-direction is not sensitive to the measurement results. This provides the accuracy of a resonator technique without machining the sample. The uncertainty of the permittivity measurements of a sample of thickness h is $\Delta\epsilon/\epsilon = \pm(0.0015 + \Delta h/h)$, and uncertainty in loss tangent measurement is $\Delta(\tan \delta) = 2 \times 10^{-5}$. The sample dimensions required for SPDR operating at 5.155 GHz are $50 \times 50 \times 1.8 \text{ mm}^3$.

Table 4 gives the dielectric properties measured at 1 MHz and moisture absorption of BR/AL and BR/nAL composites. The relative permittivity of both composites increases with filler loading. This is due to the high relative permittivity of alumina compared to butyl rubber matrix. From Table 4, it is clear that the composite with nanoalumina has higher relative permittivity than that with micron alumina. The composites filled with nanoparticles have large interfacial area for the same filler loading which promotes interfacial polarization mechanism leading to higher relative permittivity of BR–nanoalumina composites. The loss tangent is the main factor affecting the frequency selectivity of a material and is influenced by many factors such as porosity, microstructure, and defects [23]. The loss tangent of both composites shows same trend as that of relative permittivity.

Fig. 4 Variation of **a** relative permittivity and **b** loss tangent of BR/AL and BR/nAL composites at 5 GHz [22]

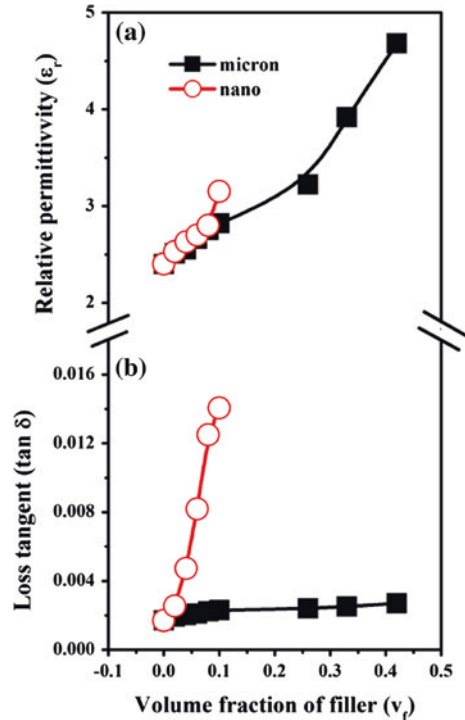


Figure 4a, b [22] shows the variation of relative permittivity and loss tangent of BR–nanoalumina and BR–micron alumina composites at 5 GHz. As the relative permittivity of alumina is higher than that of butyl rubber, the ϵ_r of BR/AL composite and BR/nAL composite show an increasing trend with filler content. The nanoalumina-filled butyl rubber composites have higher relative permittivity than micron composites. Similar behavior was observed in PTFE–silica, PTFE–rutile, and PEEK–SrTiO₃ composites [34–36]. It was reported that the nanofiller has more polarization at interface region due to its high surface area and also due to its large interface region between the filler and matrix. The nanocomposites also have higher moisture content due to its large surface area. These factors will contribute to the higher relative permittivity of nanocomposites. The relative permittivity of BR/AL composite increases from 2.40 to 4.68 as the micron alumina content increases from 0 to 0.42 v_f and that of BR/nAL composite from 2.40 to 3.15 when the nanoalumina loading increases from 0 to 0.1 v_f . It is also noted that the loss tangent increases with the increase in filler content of both micron and nanosized alumina and a higher loss tangent is exhibited by the nanoalumina-filled composites. The main reason for the higher loss tangent of nanocomposite is due to its high moisture content. A similar observation was reported in PTFE/rutile, epoxy/SiO₂, and PTFE/alumina composites [35, 37, 40]. The loss tangent of BR–micron alumina composite increases from 0.0017 to 0.0027

Table 5 Dielectric properties at 1 MHz and water absorption of BR/BT and BR/nBT composites [20]

Composite material	Sample designation	Filler in phr [#] ([§])	ϵ_r (1 MHz)	$\tan \delta$ (1 MHz)	Water absorption (vol.%)
Butyl rubber–micron BaTiO ₃ composites	BR-0	0 (0.00)	2.44	0.0003	0.039
	BR/BT-1	10 (0.02)	2.56	0.0009	0.040
	BR/BT-2	25 (0.04)	2.74	0.0011	0.045
	BR/BT-3	50 (0.07)	3.14	0.0015	0.046
	BR/BT-4	100 (0.13)	3.88	0.0016	0.048
	BR/BT-5	200 (0.24)	6.06	0.0020	0.057
	BR/BT-6	300 (0.32)	7.94	0.0021	0.068
	BR/BT-7	400 (0.38)	9.18	0.0023	0.120
Butyl rubber–nano BaTiO ₃ composites	BR/nBT-1	10 (0.02)	2.63	0.0022	0.048
	BR/nBT-2	25 (0.04)	2.86	0.0033	0.052
	BR/nBT-3	50 (0.07)	3.37	0.0077	0.059
	BR/nBT-4	100 (0.13)	4.39	0.0080	0.078
	BR/nBT-5	200 (0.24)	7.02	0.0110	0.091

[#]Parts per hundred rubber

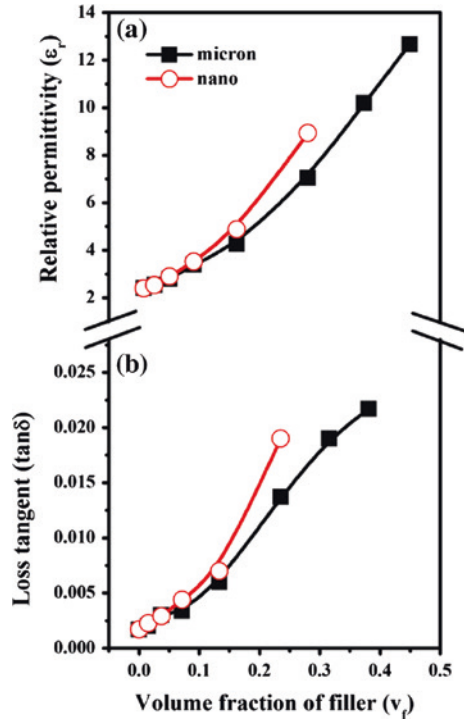
[§]The corresponding ceramic volume fraction is given in parenthesis

as the ceramic loading increases from 0 to 0.42 v_f and that of BR–nanoalumina composite increases from 0.0017 to 0.0140 as the nanoalumina content increases from 0 to 0.1 v_f at 5 GHz.

The dielectric properties at 1 MHz and water absorption values of both butyl rubber–micron BaTiO₃ and butyl rubber–nano BaTiO₃ composites are given in Table 5. The relative permittivity and loss tangent of both BR/BT and BR/nBT composites show an increasing trend with ceramic content since the relative permittivity and loss tangent of BaTiO₃ are higher than those of butyl rubber matrix. The relative permittivity and loss tangent of nano-based composites are higher than those of the micron-based composites for the same volume fraction of the filler.

Figure 5a shows the variation of relative permittivity of BR/BT and BR/nBT composites with ceramic content at 5 GHz. The ϵ_r of both composites shows the same trend as at 1 MHz. The nano-BaTiO₃-filled butyl rubber composite shows higher relative permittivity than micron-based composites due to the presence of higher moisture content in the nanocomposite since the relative permittivity of water is high ($\epsilon_r \sim 80$). The interface region between the filler and matrix is large in the case of nanocomposites which can also contribute to higher relative permittivity [34]. The relative permittivity of BR/BT composite is 7.03 for ceramic loading of 0.24 v_f and that of BR/nBT composite is 8.79 for the same loading of nano-BaTiO₃. Although ϵ_r of BaTiO₃ is much higher than that of matrix, the composite cannot attain higher relative permittivity. The relative permittivity of polymer–ferroelectric ceramic composite cannot increase to a very high value even at maximum filler loading [38] since the 0–3 type composite follows an exponential relationship between relative permittivity of composite and the volume fraction

Fig. 5 Variation of **a** relative permittivity and **b** loss tangent of BR/BT and BR/nBT composites at 5 GHz [20]



of the filler. Logarithm of the relative permittivity of such composites ($\epsilon'_{\text{composite}}$) is linearly proportional to the volume fraction of the filler (ϕ_{filler}) with the slope dependent on the dielectric properties of both components:

$$\log \epsilon'_{\text{composite}} = \phi_{\text{filler}} \log \left(\epsilon'_{\text{filler}} / \epsilon'_{\text{polymer}} \right) + \log \epsilon'_{\text{polymer}} \quad (6)$$

In general, it is difficult to prepare polymer composite with ceramic loading higher than 0.40 v_f . In order to get a polymer composite with relative permittivity higher than 100 based on typical polymers with relative permittivity of the order of 5, the relative permittivity of the filler must be higher than 9000 [38]. Xie et al. [39] prepared core-shell-structured polymethylmethacrylate–BaTiO₃ nanocomposites by in situ atom transfer radical polymerization of methyl methacrylate from the surface of BaTiO₃ nanoparticles. For 76.88 wt% of BaTiO₃ content, the composite achieved ϵ_r of 14.6 and $\tan \delta$ of 0.00372 at 1 kHz [39]. The addition of ceramic fillers gradually increased the relative permittivity. The increase in the relative permittivity depends on the amount of ceramic filler, its relative permittivity, and the frequency of measurement.

The variation of loss tangent of both BR/BT and BR/nBT composites with filler loading is also shown in Fig. 5b. The loss tangent of both composites increases with filler volume fraction since the loss tangent of BaTiO₃ is higher than that of butyl rubber. The $\tan \delta$ of butyl rubber–nanobarium titanate composite is higher

than that of butyl rubber–micron barium titanate composites. This is due to the presence of higher moisture content in the nanocomposites, larger surface area, and reactivity of nanoparticles. The presence of large amount of grain boundaries and structural defects like lattice strain can also increase the loss tangent of nanocomposites [40]. The $\tan \delta$ of micron composite is 0.0140 for a filler loading of 0.24 v_f and that of nanocomposite is 0.0190 for the same filler loading.

3.1 Theoretical Modeling of Relative Permittivity

The prediction of effective relative permittivity of polymer–ceramic composites is very important for engineering applications. In order to understand the physical mechanisms controlling the relative permittivity of a heterogeneous system, the experimental values of ϵ_r were compared with values predicted using different theoretical models. Several numerical relations have been proposed to predict the relative permittivity of polymer–ceramic composites [41–47]. These models can also be used to determine the extent of filler dispersion and filler/matrix compatibility by comparing the predicted values with the experimental data. The relative permittivity of the composites is influenced not only by the relative permittivity of the individual components but also by other factors such as morphology, porosity, the presence of moisture, impurities, agglomerates, mechanical and chemical coupling between rubber and filler, and dispersion and interaction between the two phases [21, 37, 39, 47–51], and hence, the prediction of relative permittivity of composites is very difficult. The following equations are used to predict the relative permittivity of the rubber–ceramic composites theoretically:

(a) Lichtenecker's equation:

The most widely used relation for the prediction of ϵ_r is Lichtenecker's logarithmic law of mixing. It considers the composite system as randomly oriented spheroids that are uniformly distributed in a continuous matrix [44].

$$\ln \epsilon_{\text{eff}} = (1 - v_f) \ln \epsilon_m + v_f \ln \epsilon_f \quad (7)$$

where ϵ_{eff} , ϵ_f , and ϵ_m are the relative permittivity of the composites, filler, and matrix, respectively, and v_f is the volume fraction of the filler.

(b) Maxwell-Garnett equation:

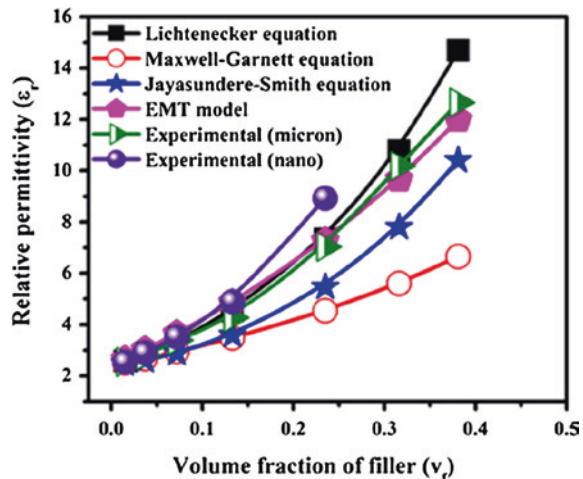
The Maxwell-Garnett mixing rule was initially used to calculate the effective permittivity of a system where metal particles are encapsulated in an insulating matrix. This mixing rule was modified for polymer–ceramic composites incorporating homogeneous distribution of spherical ceramic particles, and the excitation of dipolar character is considered [45].

$$\frac{\epsilon_{\text{eff}} - \epsilon_m}{\epsilon_{\text{eff}} + 2\epsilon_m} = v_f \frac{\epsilon_f - \epsilon_m}{\epsilon_f + 2\epsilon_m} \quad (8)$$

with the experimental values of ϵ_r of both BR/AL and BR/nAL composites up to $0.1 v_f$. In Maxwell-Garnett model, only the excitation of dipolar character is considered to be important and the correlations between these excitations are not taken into account. The multipolar contributions to the local field are also neglected. It may be noted that these assumptions are valid only in dilute systems [46]. Hence, the Maxwell-Garnett model shows deviation at higher filler content. The most widely used relation for the prediction of ϵ_r is Lichtenecker's logarithmic law of mixing [44]. The deviation of experimental values of ϵ_r of both composites from Lichtenecker's equation at higher filler loadings may be due to the lack of consideration of interfacial interaction between the polymer and the filler particles. The EMT model is also in agreement with experimental values of ϵ_r of both composites at lower filler loadings and shows deviation at higher filler content. The experimental values of ϵ_r of both composites are matching with those values calculated from Jayasundere–Smith equation and show deviation at higher filler loadings. It is found that EMT and Maxwell-Garnett models are matching more with experimental results. The deviation of all theoretical models at higher filler loading is due to the imperfect dispersion of filler particles in the butyl rubber matrix. The effective permittivity of a composite depends on the various factors such as relative permittivity of individual components in the system, their volume fractions, shape, size, porosity, interphase polarizability, and interphase volume fractions. All these parameters cannot be accounted in a single equation. Hence, the experimental results show deviation from the theoretical values at higher filler content.

Figure 7 compares the experimental and theoretical relative permittivities at 5 GHz for both butyl rubber–micron BaTiO₃ and butyl rubber–nano-BaTiO₃ composites. The experimental values of ϵ_r of both BR/BT and BR/nBT composites are in agreement with Lichtenecker's equation and EMT model at low filler loadings. The ϵ_r of BR/BT composites shows deviation from both models above a filler loading of $0.24 v_f$ of BaTiO₃ content. The relative permittivity of BR/nBT

Fig. 7 Comparison between experimental and theoretical relative permittivity of BR/BT and BR/nBT composites at 5 GHz [20]



composites is matching more with Lichtenecker’s equation and EMT models. The deviation at higher filler loading may be due to the inhomogenous dispersion of nanofiller particles in the rubber matrix.

3.2 Temperature Coefficient of Relative Permittivity (τ_{ϵ_r})

The relative permittivity of a material should be stable within the operational temperature range of electronic devices for practical applications. The temperature coefficient of relative permittivity of the present composites was measured by parallel plate capacitor method. The sample is kept in a chamber, and ϵ_r is measured from 25 to 75 °C.

Figure 8a, b shows the temperature dependence of relative permittivity of BR/nAL and BR/AL composites, respectively. From the figure, it is clear that all

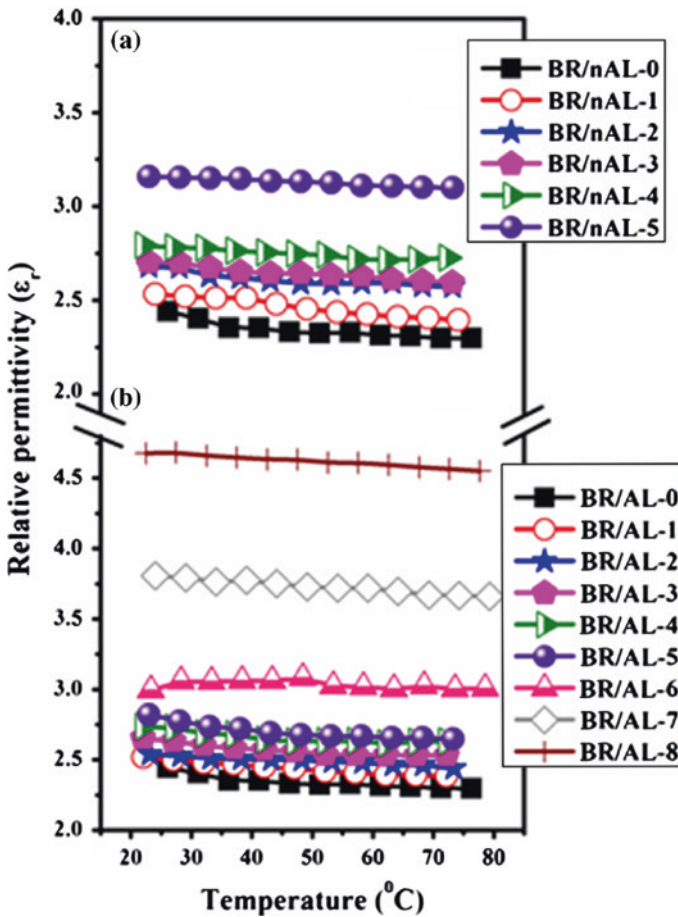


Fig. 8 Variation of relative permittivity of a BR/nAL and b BR/AL composites with temperature [22]

the composites are almost thermally stable within the measured temperature range. Figure 9a, b shows the temperature variation of relative permittivity of both BR/nBT and BR/BT composites at 1 MHz, respectively. The relative permittivity of all the composites of butyl rubber–micron BaTiO₃ and butyl rubber–nano-BaTiO₃ is also nearly stable in the measured temperature range. From the Figs. 8 and 9, it is clear the relative permittivity of composites shows a slight decrease with increase in temperature. The small decrease in relative permittivity with temperature may be due to the large difference in thermal expansion coefficient of butyl rubber and the ceramics [52, 53]. The thermal stability of relative permittivity is one of the important properties of the substrate materials that control the overall performance of the device.

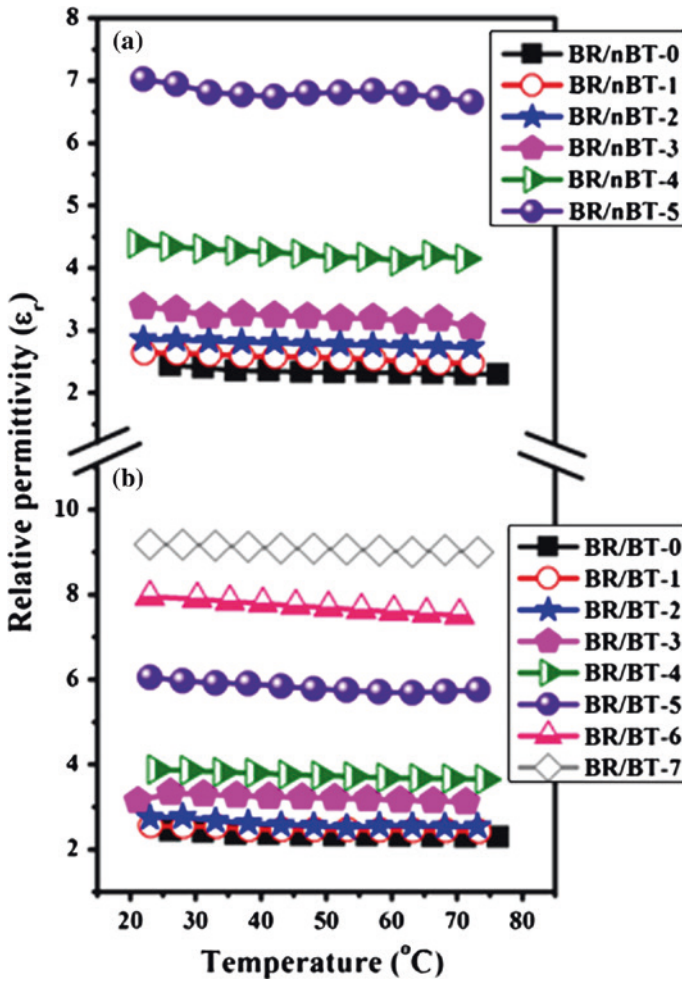


Fig. 9 Variation of relative permittivity of a BR/nBT and b BR/BT composites with temperature at 1 MHz [20]

3.3 Bending

The bending effect on dielectric properties is important as far as flexible electronic applications are concerned. Bending measurements of the composites were carried out by bending the samples manually in such a way that every part of the sample had undergone 180° bending. The bending cycle was repeated for 125 times, and the microwave dielectric properties were measured by SPDR method after every 25 cycles. Figures 10 and 11 show the variation of dielectric properties of BR/AL and BR/nAL composites with bending. It is clear from Fig. 11a, b that the relative permittivity of all the composites is nearly independent of bending. It is evident from Fig. 10a, b that the loss tangent of the nanocomposites is almost independent of bending and that of micron composite shows slight variation with bending. Figures 12 and 13 show the effect of bending on dielectric properties

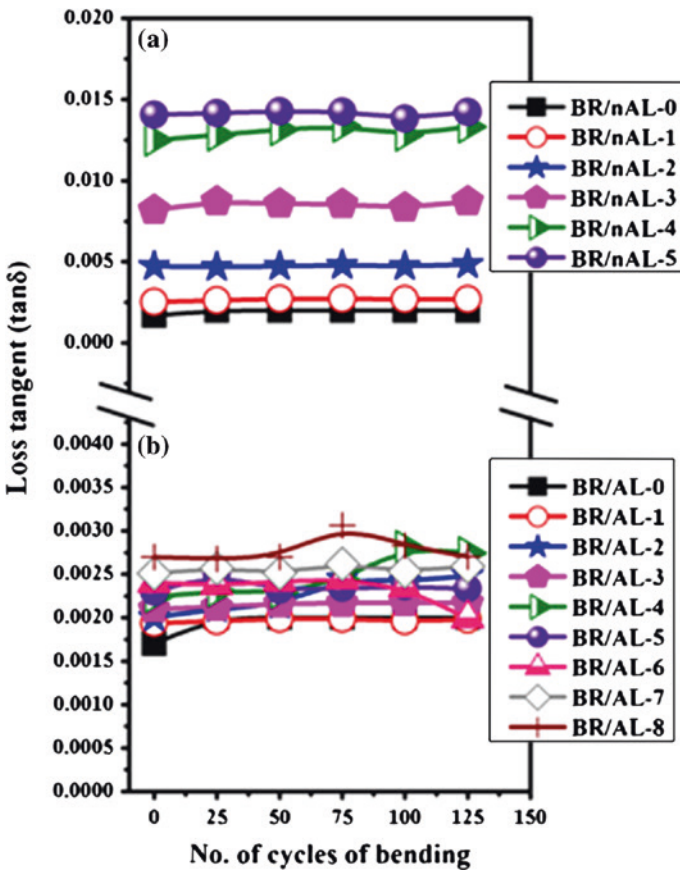


Fig. 10 Variation of relative permittivity of a BR/nAL and b BR/AL composites with bending [22]

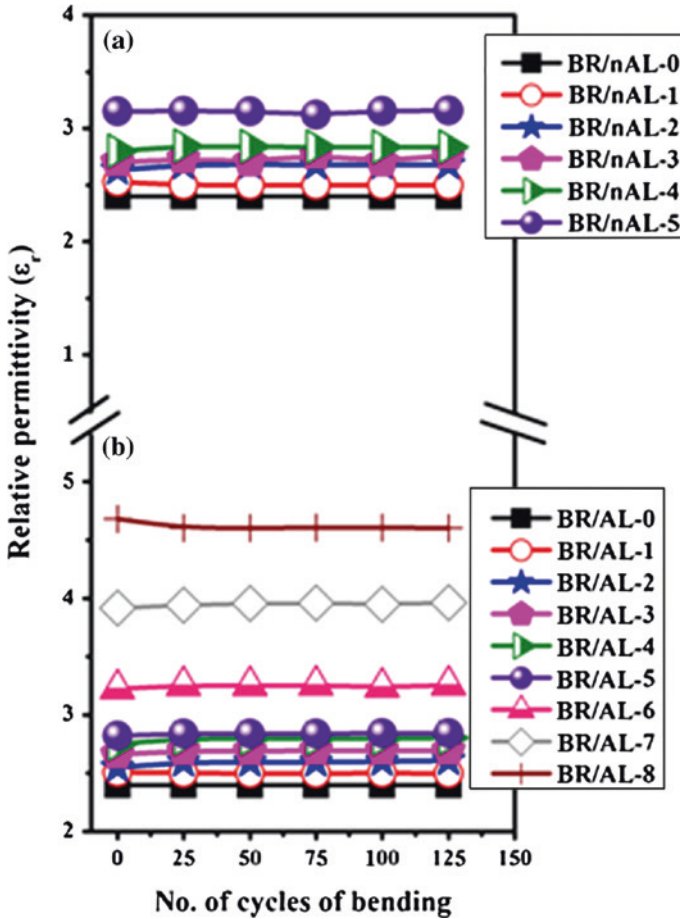


Fig. 11 Variation of loss tangent of a BR/nAL and b BR/AL composites with bending [22]

of BR/BT and BR/nBT composites at 5 GHz. The relative permittivity of both composites is almost independent of bending as is evident from Fig. 13a, b. The loss tangent of both BR/BT and BR/nBT composites shows a slight variation in mechanical bending, but the variations are marginal. Vrejoiu et al. [54] observed a similar behavior in PFCB (perfluorocyclobutene (poly 1,1,1-triphenyl ethane per-fluorocyclobutyl ether)–BaTiO₃ composites. They observed that repeated mechanical bending up to 50 cycles does not change ϵ_r and $\tan \delta$ of the composites. The bending of the composites does not considerably affect the microwave dielectric properties, and hence, they are suitable for flexible electronic applications.

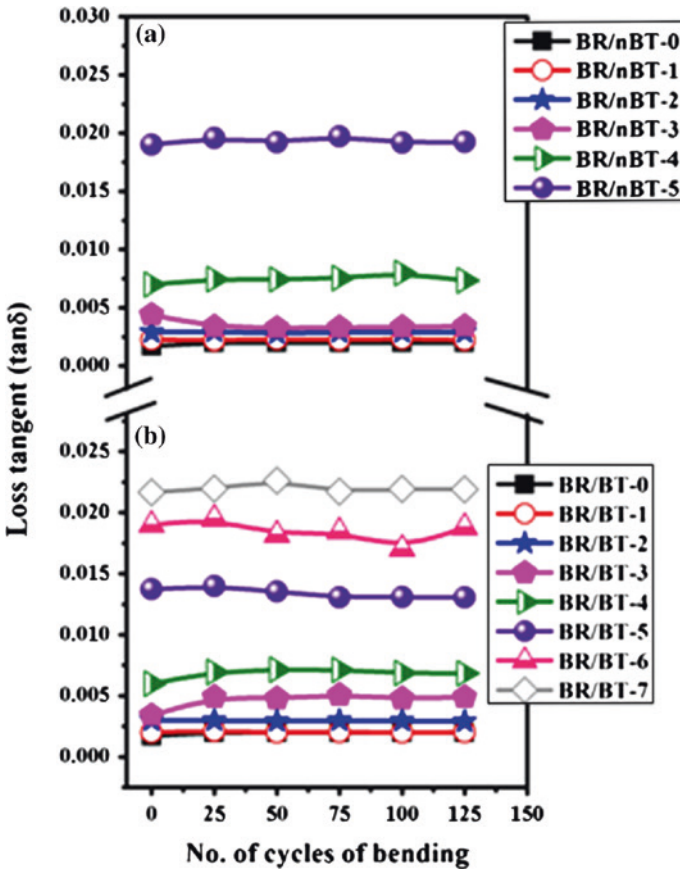


Fig. 12 Variation of relative permittivity of a BR/nBT and b BR/BT composites with bending [20]

4 Thermal Conductivity

Heat dissipation from integrated circuits is a crucial problem for electronic industry that affects potential miniaturization, speed, and reliability. The thermal conductivity (TC) of polymers is very low, ranging from 0.14 to 0.60 W m⁻¹ K⁻¹ [55], and can be improved by the addition of ceramic fillers as the TC of ceramic is higher than that of polymers. The TC of the composites depends on the intrinsic thermal conductivities of filler and matrix, shape and size of the filler, and the loading level of filler [56]. The variation of TC of both BR/AL and BR/nAL composites with filler content is shown in Fig. 14. The TC of both composites shows increasing trend with ceramic loading. This is quite expected since the TC of alumina (30 W m⁻¹ K⁻¹) is higher than that of butyl

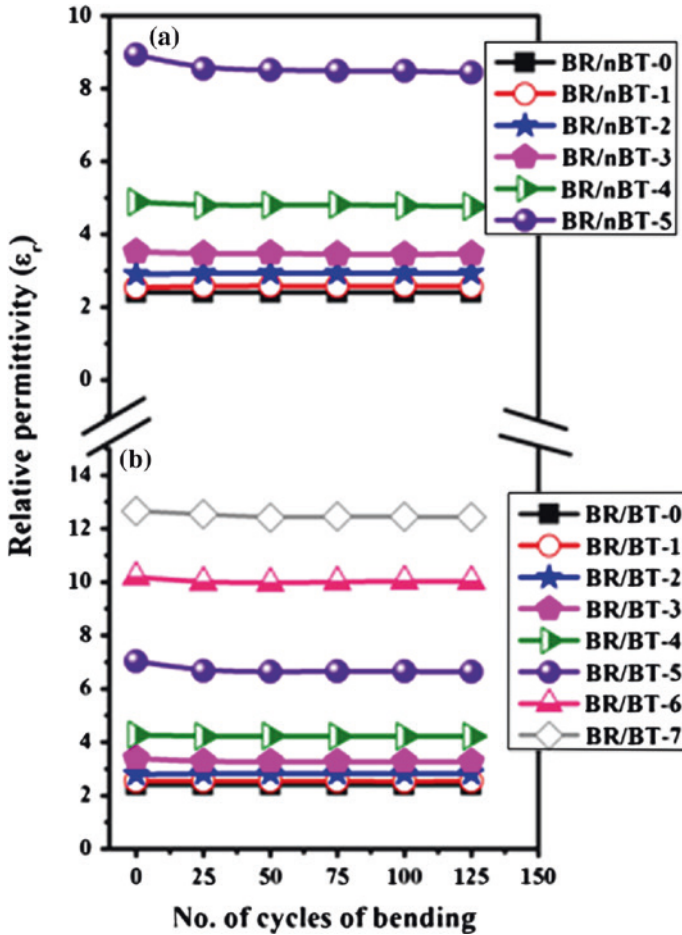


Fig. 13 Variation of loss tangent of a BR/nBT and b BR/BT composites with bending [20]

rubber matrix ($0.13 \text{ W m}^{-1} \text{ K}^{-1}$). From the inset plot in Fig. 14 [22], it is clear that the TC of nanoalumina-loaded composites is slightly higher than that of micron composite.

Figure 15 shows the variation of TC of BR/BT and BR/nBT composites with ceramic loading. As the ceramic loading increases, the TC of both composite increases since the TC of BaTiO_3 ($2.6 \text{ W m}^{-1} \text{ K}^{-1}$) is higher than the butyl rubber ($0.13 \text{ W m}^{-1} \text{ K}^{-1}$). As the filler loading increases, distance between the filler particles decreases and thus filler becomes the main channels for thermal conduction. Hence, TC of both composites can also increase with filler content [56]. From Figs. 14 and 15, it is clear that the nanocomposites have higher TC than that of

Fig. 14 Variation of thermal conductivity of BR/AL and BR/nAL composites with filler content [22]

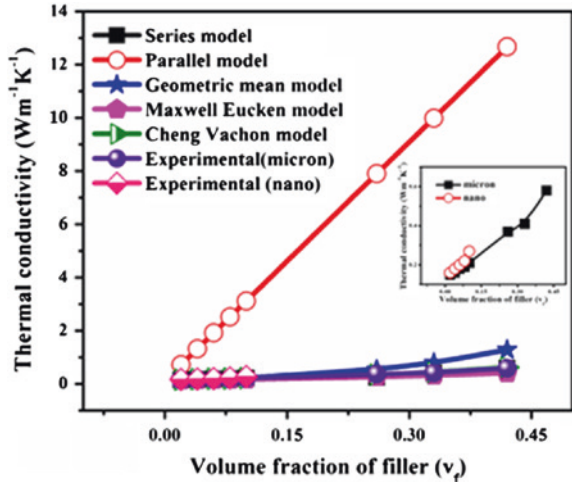
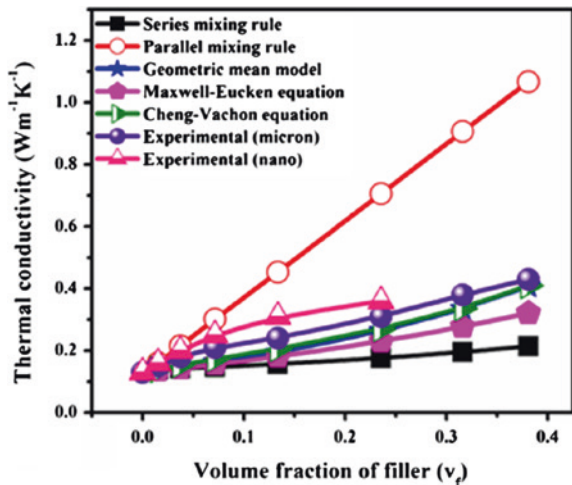


Fig. 15 Variation of thermal conductivity of BR/BT and BR/nBT composites with filler content [20]



micron-based composites. The matrix/filler interface plays a critical role in nano-composites due to its large surface area. The number of particles increases with decreasing particle size for the same filler content [57, 58]. This will lead to the formation of a large number of heat-conductive channels in nanofiller-added composites. Hence, the TC of nano-based composite is higher than micron-based composites. The butyl rubber–micron barium titanate composite with ceramic loading of 0.24 v_f has a TC of $0.31 \text{ W m}^{-1} \text{ K}^{-1}$ and that of butyl rubber–nanobarium titanate composite is $0.36 \text{ W m}^{-1} \text{ K}^{-1}$.

4.1 Theoretical Modeling of Thermal Conductivity

The effective TC of a heterogeneous system is strongly affected by its TC of individual components, composition, crystal structure, distribution within the medium, and contact between the particles. Numerous theoretical models were proposed for predicting the TC of composites [59, 60]. The following models are used to predict the TC of the composites:

(a) **Series mixing rule:**

$$\frac{1}{k_c} = \frac{v_f}{k_f} + \frac{v_m}{k_m} \quad (11)$$

where k_c is the effective TC of the composite, k_m and k_f are the TC of matrix and filler, respectively, and v_m and v_f are the volume fractions of matrix and filler, respectively.

(b) **Parallel mixing rule:**

$$k_c = v_f k_f + v_m k_m \quad (12)$$

The physical structures assumed in the series and parallel models are of layers of phases aligned either perpendicular or parallel to the heat flow [59]. The series and parallel model of TC gives only lower and upper limits of TC values of composites, respectively.

(c) **Geometric mean model [60]:**

$$k_c = k_f^{v_f} k_m^{1-v_f} \quad (13)$$

(d) **Maxwell-Eucken Model:**

$$k_c = k_m \left[\frac{k_f + 2k_m + 2V_f(k_f - k_m)}{k_f + 2k_m - V_f(k_f - k_m)} \right] \quad (14)$$

The Maxwell model assumes a dispersion of small spheres within a continuous matrix of a different phase, where spheres being far enough apart such that the local distortions to the temperature distributions around each of the spheres do not interfere with their neighbors' temperature distributions [60].

(e) **Cheng–Vachon Model:**

Cheng and Vachon assumed a parabolic distribution of the discontinuous phase in the continuous phase based on Tsao's model [61]. The constants of this parabolic distribution were determined by analysis and presented as a function of the discontinuous phase volume fraction. Thus, the equivalent TC of the two-phase solid mixture was derived in terms of the distribution function and the TC of the constituents.

$$\frac{1}{k_c} = \frac{1}{\sqrt{C}(k_f - k_m)[k_m + B(k_f - k_m)]} \ln \frac{\sqrt{[k_m + B(k_f - k_m)] + \frac{B}{2}\sqrt{C}(k_f - k_m)}}{\sqrt{[k_m + B(k_f - k_m)] - \frac{B}{2}\sqrt{C}(k_f - k_m)}} + \frac{1 - B}{k_m} \quad (15)$$

where

$$B = \sqrt{3V_f/2} \quad C = -4\sqrt{2/3V_f} \quad (16)$$

Figure 14 also compares the experimental TC of both BR/AL and BR/nAL composites with theoretical models. The series and parallel model of TC gives only lower and upper limits of TC values of composites, respectively [59]. The experimental TC values of both composites are within the range of series and parallel model. The geometric mean model is in good agreement with experimental TC of both composites up to a volume fraction of 0.1 and has a lower value than predicted TC at higher micron alumina loading. This may be due to the agglomeration of filler particles at higher filler loadings. The models Cheng–Vachon and Maxwell-Eucken are matching with experimental TC of both composites. Figure 15 also shows the comparison between experimental and theoretical TC of BaTiO₃-based composites. The series and parallel mixing rule of both composites shows the same trend as that of alumina-based composites and does not match with experimental profiles. All the other theoretical models are matching with TC of BR/nBT composites at low filler loading and show deviation at higher nano-BaTiO₃ content. The TC of butyl rubber–micron BaTiO₃ composites is in agreement with Cheng–Vachon and geometric mean models. Maxwell-Eucken equation holds good at low filler loading and deviates at higher micron BaTiO₃ content [62].

5 Mechanical Properties

The mechanical flexibility is the prime requirement for flexible electronic applications. Tensile test is useful to evaluate mechanical properties of materials in which the sample is pulled to failure in a relatively short period of time. The sample is elongated at a constant rate, and the load required to produce a given elongation is measured as a dependent variable. A stress–strain curve may be plotted from the results of a tension test, and from the plot, the toughness of the material can be assessed [63, 64]. The stress–strain properties of the composites were measured using a universal testing machine (Hounsfield, H5K-S UTM, Redhill, U.K.) with a rate of grip separation of 500 mm/min. Tensile tests were conducted using dumb-bell-shaped samples of width 4 mm and thickness in the range 1.5–2 mm.

Figure 16 shows the stress–strain curve of BR/AL and BR/nAL composites. The mechanical properties of a particulate composite depend on the strength of the adhesive bond between the different phases, the type of dispersion, and the amount of particle agglomeration. From the figure, it is clear that the stress needed for ceramic-filled butyl rubber composite is greater than that of unfilled sample. Among BR-0, BR/AL-5, and BR/nAL-5, the stress required for BR/nAL-5 composite is high. This may be due to more homogeneous dispersion of nanoparticles in the rubber matrix. Chee et al. [65] reported that at lower filler loading, the nanoalumina particle orients along the direction of stress and this would reinforce and increase the stiffness of the

Fig. 16 Stress–strain curves of BR/AL and BR/nAL composites [19]

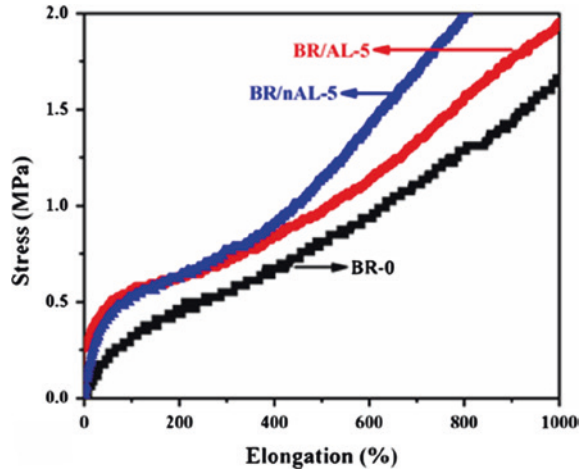
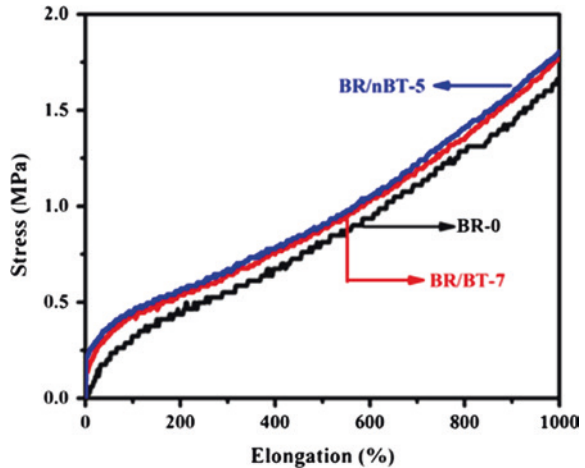


Fig. 17 Stress–strain curves of BR/BT and BR/nBT composites [20]



nanocomposite. Figure 17 shows the stress–strain curves of BR/BT-7 and BR/nBT-5. As the filler loading increases, the stress needed for elongation and also stiffness of the composite increases [66]. This figure shows that the nanocomposite is slightly stiffer than micron composite. Both the composites were not broken up to an elongation of 1000 %, which indicates the excellent mechanical flexibility of the composites.

6 Moisture Absorption of Composites

The moisture content is an important parameter for materials used for practical applications. Absorption of moisture from the working atmosphere will degrade the dielectric properties since water is a polar molecule. The moisture absorption

characteristics of the composites were measured using the samples with dimensions 50 mm × 50 mm × 2 mm. The samples were weighed accurately and immersed in distilled water for 24 h. The samples were then taken out and again weighed after removing the excess water from the surface. The volume % of water absorption was then calculated using the relation,

$$\text{Volume \% water absorption} = \frac{(W_f - W_i)/\rho_w}{(W_f - W_i)/\rho_w + W_i/\rho_c} \times 100 \quad (17)$$

where W_i and W_f are the initial and final weights of the sample, and ρ_w and ρ_c are the densities of distilled water and composite, respectively.

It is evident from Tables 4 and 5 that as the filler content increases, the volume % (vol.%) of water content increases for both composites since the ceramic is hydrophilic in nature. Compared to micron composite, nanocomposites have a high tendency to absorb moisture due to the large surface area of the nanoalumina or barium titanate, and also, higher nanofiller loading leads to the formation of pores in the composites due to the agglomeration of the particles. The loss tangent and moisture absorption of butyl rubber–nanoceramic composites are much higher as compared to the micron composites. The dielectric properties of the composites are affected by the presence of moisture content. The absorbed moisture interacts with polymer matrix and also with the filler–matrix interface [67] and thus affects the dielectric properties of composites.

7 Coefficient of Thermal Expansion

Figures 18 and 19 show the variation of coefficient of thermal expansion (CTE) of butyl rubber–alumina and barium titanate composites with filler content. The CTE of both the composites decreases with ceramic loading since

Fig. 18 Variation of CTE of BR/AL and BR/nAL composites with filler content [19]

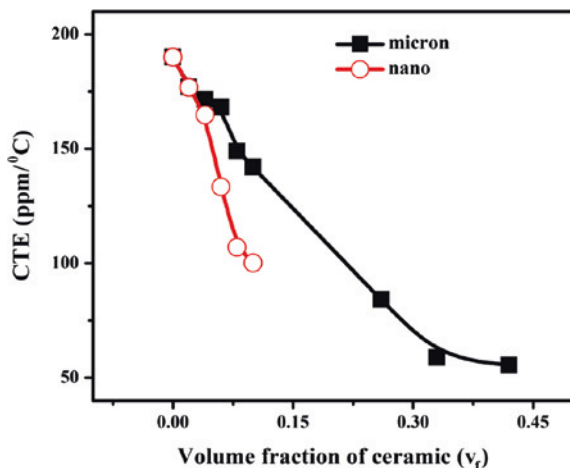
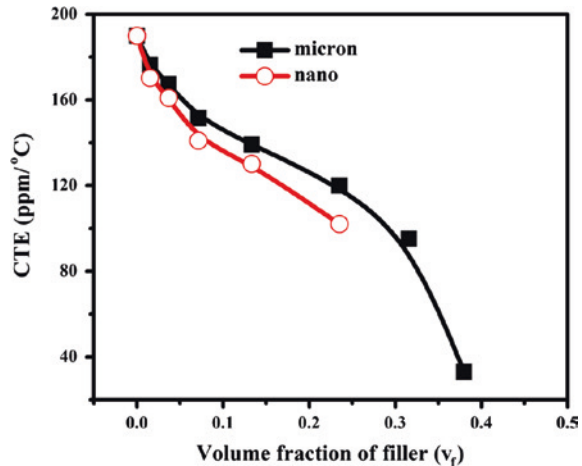


Fig. 19 Variation of CTE of BR/BT and BR/nBT composites [20]



the CTE value of the ceramics is smaller than that of rubber matrix, and also, the mobility of loose molecular bonds in the polymer chains is restrained by the ceramic loading [68, 69]. The BR–nanocomposites show much lower CTE value compared to that of micron composites. The physical cross-linking points are more in the case of nanoparticles because of its high specific surface area, and this will increase the mechanical interaction between the filler and rubber matrix [70]. Hence, the nanocomposites have lower CTE than that of micron composites.

8 Conclusions

The butyl rubber–ceramic composites can be prepared by sigma mixing followed by hot pressing. The composites were found to be flexible, bendable, and stretchable. The microwave dielectric and thermal properties are improved with ceramic loading. The composite preparation is difficult for ceramic loading higher than 40 vol.%. The nanopowder can be loaded to a much lower level. The relative permittivity essentially depends on the rubber matrix, and one can get a relative permittivity of about 15 even with maximum loading with high-permittivity ceramics. The TC of the composites increased and CTE decreased with ceramic content. The water absorption increases with increase in ceramic loading and is higher for nanoceramic loading. The composite with nanoceramic filler has inferior microwave dielectric properties. Table 6 gives the microwave dielectric properties of several butyl rubber–ceramic composites. The BR/AL and BR/BT composites are found to be suitable candidates for microwave substrate and electronic packaging applications. More recently, butyl rubber–single-walled carbon nanotube (BR-SWCNT) composites were prepared by a solution mixing process

Table 6 Microwave dielectric, thermal, and physical properties of several butyl rubber–ceramic composites [22]

Filler	v_f of filler	ϵ_r	$\tan \delta$	TC ($W\ m^{-1}\ K^{-1}$)	CTE (ppm/ $^{\circ}C$)	Water absorption (vol.%)
SiO ₂	0.40	3.09	0.0045	0.56	80	0.09
Al ₂ O ₃	0.40	4.68	0.0027	0.58	55	0.08
Ba(Zn _{1/3} Ta _{2/3})O ₃	0.32	5.72	0.0025	0.35	86	0.05
TiO ₂	0.40	12.5	0.0027	0.72	108	0.08
Sr ₂ Ce ₂ Ti ₅ O ₁₅	0.43	11.0	0.0018	0.49	30	0.07
SrTiO ₃	0.42	13.2	0.0028	0.55	26	0.08
BaTiO ₃	0.38	12.7	0.0200	0.43	33	0.12
Ba _{0.7} Sr _{0.3} TiO ₃	0.39	13.1	0.0090	0.41	29	0.06

and reported to be useful EMI shielding applications. The BR-SWCNT composite shows enhanced relative permittivity of 14 with a loss tangent of 0.07 at 15 GHz for 8 phr SWCNT [71]. The EMI shielding effect increased with SWCNT content.

References

- Gargama H, Thakur AK, Chaturvedi SK (2015) Polyvinylidene fluoride/nickel composite materials for charge storing, electromagnetic interference absorption, and shielding applications. *J Appl Phys* 117: 224903-1-9
- Sudeep PM, Vinayasree S, Mohanan P, Ajayan PM, Narayanan TN, Anantharaman MR (2015) Fluorinated graphene oxide for enhanced S and X-band microwave absorption. *Appl Phys Lett* 106:221603-1–221603-5
- Siegel AC, Phillips ST, Dickey MD, Lu N, Suo Z, Whitesides GM (2010) Foldable printed circuit boards on paper substrates. *Adv Funct Mater* 20:28–35
- Kim DH, Rogers JA (2008) Stretchable electronics: materials, strategies and devices. *Adv Mater* 20:4887–4892
- Kramer RK, Majidi C, Sahai R, Wood RJ (2011) IEEE/RSJ international conference on intelligent robots and systems, San Francisco, CA, USA, 25–30 September 1919–1926
- Seol YG, Noh HY, Lee SS, Ahn JH, Lee NE (2008) Mechanically flexible low-leakage multilayer gate dielectrics for flexible organic thin film transistor. *Appl Phys Lett* 93:013305-1–013305-3
- Sebastian MT, Jantunen H (2010) Polymer-ceramic composites of 0-3 connectivity for circuits in electronics: a review. *Int J Appl Ceram Technol* 7:415–434
- Thomas RM, Sparks WJ (1944) Mixed olefinic polymerization process and product. U.S. patent, 2, 356, 128
- http://en.wikipedia.org/wiki/Butyl_rubber
- Ebewele RO (2000) Polymer science and technology. CRC Press, Florida
- <http://en.wikipedia.org/wiki/Elastomer>
- Billmeyer FW (1962) Text book of polymer science. Interscience Publishers, Wiley, New York, London
- Duffy J, Wilson GJ (1993) Synthesis of butyl rubber by cationic polymerization. In: Ullman's encyclopedia of industrial chemistry, 5th edn. Elsevier, Amsterdam
- General properties of elastomers, www.elbex-us.com

15. Thomas D, Chameswary J, Sebastian MT (2011) Mechanically flexible butyl rubber-SrTiO₃ composites for microwave applications. *Int J Appl Ceram Technol* 8:1099–1107
16. Chameswary J, Thomas D, Subodh G, Harshan S, Philip J Sebastian MT (2012) Microwave dielectric properties of flexible butyl rubber-strontium cerium titanate composites. *J Appl Polym Sci* 124:3426–3433
17. Chameswary J, Sebastian MT (2013) Effect of Ba(Zn_{1/3}Ta_{2/3})O₃ and SiO₂ ceramic fillers on the microwave dielectric properties of butyl rubber composites. *J Mater Sci: Mater Electron* 24:4351–4360
18. Chameswary J, Sebastian MT (2013) Butyl rubber-Ba_{0.7}Sr_{0.3}TiO₃ composites for flexible microwave electronic applications. *Ceram Int* 39:2795–2802
19. Chameswary J, Namitha LK, Brahmakumar M, Sebastian MT (2014) Material characterization and microwave substrate applications of alumina filled butyl rubber composites. *Int J Appl Ceram Technol* 11:919–926
20. Chameswary J, Sebastian MT (2015) Preparation and Properties of BaTiO₃ filled butyl rubber composites flexible electronic circuit applications. *J Mater Sci: Mater Electron*. doi:10.1007/s10854-015-2879-5
21. Chameswary J, Sebastian MT (2014) Development of butyl rubber-rutile composites for flexible microwave substrate applications. *Ceram Int* 40:7439–7448
22. Janardhanan C (2015) Butyl rubber-ceramic composites for flexible electronic applications. Ph.D thesis, Cochin University of Science & Technology
23. Sebastian MT (2008) Dielectric materials for wireless communication. Elsevier, Amsterdam
24. Mohamad N, Muchtar A, Ghazali MJ, Dahlan HM, Azhari CH (2009) Epoxidised natural rubber—alumina nanoparticle composites (ENRAN): effect of filler loading on the tensile properties. *Solid State Sci Technol* 17:133–143
25. Mohamad N, Muchtar A, Ghazali MJ, Mohd DH, Azhari CH (2008) The effect of filler on epoxidised natural rubber-alumina nanoparticles composites. *Eur J Sci Res* 24:538–547
26. Li L, Fang Y, Xiao Q, Wu YJ, Wang N, Chen XM (2014) Microwave dielectric properties of fused silica prepared by different approaches. *Int J Appl Ceram Technol* 11:193–199
27. Hanna FF, Yehiab AA, About-Bakr AF (1973) Dielectric properties of polar rubber mixtures. *Br Polym J* 5:49–53
28. Hakim IK, Bishai AM, Saad AI (1988) Dielectric properties of butyl rubber mixtures at 10⁶–10¹⁰ Hz. *J Appl Polym Sci* 35:1123–1125
29. Barron H (1949) Modern synthetic rubbers. Chapman & Hall Ltd., London
30. Hu T, Juuti J, Jantunen H, Vikkman T (2007) Dielectric properties of BST/polymer composites. *J Eur Ceram Soc* 27:3997–4001
31. Krupka J, Gregonry AP, Kochard OC, Clarke RN, Riddle B, Baker-Jarvis J (2001) Uncertainty of complex permittivity measurement by split post dielectric resonator techniques'. *J Eur Ceram Soc* 21:2673–2676
32. Krupka J, Gabelich S, Derzakowski K, Pierce BM (1999) Comparison of split post dielectric resonator and ferrite disc resonator techniques for microwave permittivity measurements of polycrystalline ytterium iron garnet. *Meas Sci Technol* 10:1004–1008
33. Krupka J (2003) Precise measurement of complex permittivity of dielectric materials at microwave frequencies. *Mater Chem Phys* 79:195–198
34. Murali KP, Rajesh S, Om Prakash A, Kulkarni R, Ratheesh R (2009) Preparation and properties of Silica filled PTFE Flexible laminates for microwave circuit applications. *Compos A* 40:1179–1185
35. Rajesh S, Nisa VS, Murali KP, Ratheesh R (2009) Microwave dielectric properties of PTFE/rutile nanocomposites. *J Alloy Compd* 477:677–682
36. Nisa VS, Rajesh S, Murali KP, Priyadarsini V, Potty SN, Ratheesh R (2008) Preparation, characterization and dielectric properties of temperature stable SrTiO₃/PEEK composites for microwave substrate applications. *Compos Sci Technol* 68:106–112
37. Todd MG, Shi FG (2002) Validation of a novel dielectric constant simulation model and the determination of its physical parameters. *Microelectron J* 33:627–632

38. Popielarz R, Chiang CK (2007) Polymer composites with dielectric constant comparable to that of barium titanate ceramics. *Mater Sci Eng B* 139:48–54
39. Xie L, Huang X, Wu C, Jiang P (2011) Core shell structured poly(Polymethyl methacrylate) nanocomposites prepared by insitu atom transfer radical polymerization: a route to high dielectric constant materials with inherent low loss of the base polymer. *J Mater Chem* 21:5897–5906
40. Murali KP, Rajesh S, Nijesh KJ, Ratheesh R (2010) The effect of particle size on the microwave dielectric properties of alumina filled PTFE substrates. *Int J Appl Ceram Technol* 7:475–481
41. Sareni B, Krahenbuh L, Beroul A, Brosseau C (1997) Effective dielectric constant of random composite material. *J Appl Phys* 81:2375–2383
42. Sihvola AH (1988) Effective permittivity of dielectric mixtures. *IEEE Trans Geosci Remote Sens* 26:420–429
43. Wakino K (1993) A new equation for predicting the dielectric constant of a mixture. *J Am Ceram Soc* 76:2588–2594
44. Goncharenko AV, Lozovski VZ, Venger EF (2000) Lichtenecker's equation: applicability and limitations. *Optics Commun* 174:19–32
45. Claro F, Rojas R (1991) Correlation and multipolar effects in the dielectric response of particulate matter: an iterative mean-field theory. *Phys Rev B* 43:6369–6375
46. Jayasundere N, Smith BV (1993) Dielectric constant for binary piezoelectric 0-3 composites. *J Appl Phys* 73:2462–2466
47. Rao Y, Qu J, Marinis T, Wong CP (2000) A precise numerical prediction of effective relative permittivity for polymer ceramic composites based on effective medium theory. *IEEE Trans Compon Packag Technol* 23:680–683
48. Teirikangas M, Juuti J, Hu T, Jantunen H (2009) Extrinsic influences of the polymer matrix on electrical properties of high frequency composites. *Ferroelectrics* 387:70–76
49. Xiang F, Wang H, Yao X (2006) Preparation and dielectric properties of bismuth based dielectric/PTFE microwave composite. *J Eur Ceram Soc* 26:1999–2002
50. Murugaraj P, Mainwaring D, Mora-Huertás N (2005) Dielectric enhancement in polymer-nanoparticle composites through interphase polarizability. *J Appl Phys* 98:054304-1–054304-6
51. Valant M, Suvorov D (2003) Microstructural phenomena in low firing ceramics. *Mater Chem Phys* 79:104–110
52. Xie SH, Zhu BK, Wei XZ, Xu ZK, Xu YY (2005) Polyimide/BaTiO₃ composites with controllable dielectric properties. *Compos A Appl Sci Manuf* 36:1152–1157
53. Berger MA, Mc Cullough RL (1985) Characterization and analysis of the electrical properties of a metal-filled polymer. *Compos Sci Technol* 22:81–106
54. Vrejoiu I, Pedarnig JD, Dinescu M, Gogonea SB, Bäuerle D (2002) Flexible ceramic-polymer composite films with temperature-insensitive and tunable dielectric permittivity. *Appl Phys A* 74:407–409
55. Tavman IH (1998) Effective thermal conductivity of isotropic polymer composites. *Int Commun Heat Mass Transfer* 25:723–732
56. Kemaloglu S, Ozkoc G, Avtak A (2010) Properties of thermally conductive micro and nano size boron nitride reinforced silicon rubber composites. *Thermochim Acta* 499:40–47
57. Zhou W, Qi S, Li H, Shao S (2007) Study on insulating thermal conductive BN/HDPE composite. *Thermochim Acta* 452:36–42
58. Ling W, Gu A, Liang G, Yuan L (2010) New composites with high thermal conductivity and low dielectric constant for microelectronic packaging. *Polym Compos* 31:307–313
59. Richerson DW (2006) Modern ceramic engineering properties. In: *Processing and use in design*. Taylor and Francis, CRC Press, London
60. Progelhof RC, Throne JL, Ruetsch RR (1976) Methods for predicting thermal conductivity of composite systems: a review. *Polym Eng Sci* 16:615–625
61. Tsao GTN (1961) Thermal conductivity of two-phase material. *Ind Eng Chem* 53:395–397

62. Jaguaribe EF, Beasley DE (1984) Modeling of the effective thermal conductivity and diffusivity of a packed bed with stagnant fluid. *Int J Heat Mass Transf* 27:399–407
63. Menard KP (1999) *Dynamic mechanical analysis: a practical introduction*. CRC Press, Boca Raton
64. Hayden HW, Moffatt WG, Wulff J (1984) The structure and properties of materials, vol III. In: *Mechanical behaviour*, Wiley Eastern Ltd., New Delhi
65. Chee CY, Song NL, Abdullah LC, Choong TSY, Ibrahim A, Chantara TR (2012) Characterization of mechanical properties: low-density polyethylene nanocomposite using nanoalumina particle as filler. *J Nanomater* 2012(215978):1–6
66. Ismail H, Sam ST, Mohd Noor AF, Bakar AA (2007) Properties of ferrite-filled natural rubber composites. *Polym Plast Technol Eng* 46:641–650
67. Zhao H, Li RKY (2008) Effect of water absorption on the mechanical and dielectric properties of nano-alumina filled epoxy nanocomposites. *Compos A Appl Sci Manuf* 39:602–611
68. Li TL, Hsu SLC (2010) Enhanced thermal conductivity of polyimide films via a hybrid of micro- and nano-sized boron nitride. *J Phys Chem B* 114:6825–6829
69. Goyal RK, Jadhav P, Tiwari AN (2011) Preparation and properties of new polyphenylene sulfide/AlN composites for electronic packaging. *J Electron Mater* 40:1377–1383
70. Zhou W, Qi S, Tu C, Zhao H, Wang C, Kou J (2007) Effect of the particle size of Al₂O₃ on the properties of filled heat-conductive silicone rubber. *J Appl Polym Sci* 104:1312–1318
71. Joseph N, Janardhanan C, Sebastian MT (2014) Electromagnetic interference shielding properties of butyl rubber single walled carbon nanotube composites. *Compos Sci Technol* 101:139–144